A Highly stretchable and conductive 3D porous graphene metal nanocomposite based electrochemical-physiological hybrid biosensor

Xing Xuan, Ji Y. Kim, Xue Hui, Partha S. Das, Hyo S. Yoon, Jae-Yeong Park

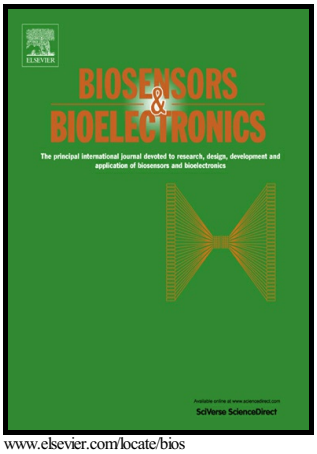

www.elsevier.com/locate/bios

PII: S0956-5663(18)30582-7
DOI: https://doi.org/10.1016/j.bios.2018.07.071
Reference: BIOS10660

To appear in: *Biosensors and Bioelectronic*

Cite this article as: Xing Xuan, Ji Y. Kim, Xue Hui, Partha S. Das, Hyo S. Yoon and Jae-Yeong Park, A Highly stretchable and conductive 3D porous graphene metal nanocomposite based electrochemical-physiological hybrid biosensor, *Biosensors and Bioelectronic,* https://doi.org/10.1016/j.bios.2018.07.071

A Highly stretchable and conductive 3D porous graphene metal nanocomposite based electrochemical-physiological hybrid biosensor

Xing Xuan, Ji Y. Kim, Xue Hui, Partha S. Das, Hyo S. Yoon, Jae−Yeong Park∗

Department of Electronic Engineering, Micro/Nano Devices & packaging Lab., Kwangwoon University, 447-1, Wolgye-Dong, Nowon Gu, Seoul, 139-701, Korea

Recently, highly stretchable and flexible electrodes essential for wearable electronic devices has been reported. However, their electrical resistances are high, the fabrication processes are complicated and involve a high cost, and deformations such as stretching can lead to the degradation on electrical performance. To address these issues, a novel fabrication process (both inexpensive and simple) for the highly stretchable and conductive electrodes using well patterned 3D porous laser-induced graphene silver nanocomposite was developed. The fabricated electrode exhibited a high, uniform electrical conductivity even under mechanical deformations. Addition of platinum and gold nanoparticles (PtAuNP) on the 3D porous LIG greatly improved the electrochemical performance for wearable glucose sensor applications. The fabricated glucose sensor exhibited low detection limit (5 μM), and acceptable detection range from 0 to 1.1 mM (covers the glucose range in sweat), and high linearity (0.99). In addition, the fabricated pH sensor also exhibited a linear response (66 mV/pH) at the range from 4 to 7. This work successfully demonstrates the potential of this novel fabrication technique and stretchable LIG metal nanocomposite for wearable electrochemical-physiological hybrid biosensors.

Key words

porous graphene-metal nanocomposite, patterning process, electrochemical-physiological sensor, flexible and stretchable electronics, wearable biosensors,

∗ Corresponding author. Tel.: +82-2-940-5113; fax: +82-2-942-1502;
e-mail: jaepark@kw.ac.kr

1. Introduction

In the last few years, research into wearable electronics (e.g., chemical and physical sensors) has evolved very rapidly due to increased demand for stretchable and flexible portable devices as alternatives to conventional rigid systems (Liu et al., 2017; Xuan et al., 2018; Maharjan et al., 2018; Kwak et al., 2017). Recently, wearable bio-sensors that can be laminated onto the surface of the skin have received tremendous attention from both academia and industry (Cai et al., 2016; Guo et al., 2017). Wearable bio-sensors can be worn or mated with human skin to continuously and closely monitor an individual's activities without interrupting or limiting the user's motions (Chen et al., 2018; Pang et al., 2018; Cho et al., 2016; Pegan et al., 2016; Yamamoto et al., 2016).

In wearable bio-sensor research area, various methods including wearable bio-sensors have been suggested for personal health monitoring in other body fluids, such as saliva, tears, and sweat (Wang et al., 2018; Bandodkar et al., 2013; Roy et al., 2017; Matzeu et al., 2015). Among these, sweat has emerged as a promising body fluid for healthcare monitoring (Moyer et al., 2011). Various kinds of flexible and wearable bio-sensors have been developed for smart bioanalysis (in human sweat) (Lee et al., 2017; Gao et al., 2016; Xuan et al., 2018; Olarte et al., 2013). However, many of these involve multiple complicated fabrication steps, which prevent mass-production and limit their broad application in wearable bio-sensors.

Recently, laser-induced graphene (LIG) has been proposed as an efficient active material for flexible and stretchable electrochemical devices (energy storage and sensors) because of its simple fabrication by one-step patterning (Lin et al., 2014; Tao et al., 2017). However, many challenges still exist for this laser graphenization process. For example, LIG has high sheet resistance after being transferred onto the stretchable substrate. Furthermore, deformations such as stretching can lead to deterioration of electrical performance. To address these issues, a novel stretchable electrode is presented here, based on a silver nanowire (AgNW)/LIG 3D network of multilayer film on a stretchable polydimethylsiloxane (PDMS) substrate. The well-patterned AgNW film between the PDMS and LIG provides a higher electrical conductivity, even under mechanical deformations, compared with previous methods (Tao et al., 2017; Li et al., 2017; Lamberti et al., 2016). Additional PtAuNP electroplating, and serpentine electrode designs, further increase electrochemical performance and deformability. The resulting stretchable electrode exhibits an improved sheet resistance, with the

resistance change under stretching (even up to around 40%) being minimal. Furthermore, the AgNW/LIG/PtAuNP hybrid stretchable electrode shows good electrochemically active properties as well. In conclusion, The Electrocardiogram (ECG), non-invasive glucose sensor (for monitoring the glucose level in blood) and pH sensor (improves the accuracy of glucose sensor) were successfully demonstrated using our improved fabrication method. The integrated biosensors are highly promising for electrochemical-physiological (Chem-Phys) hybrid sensing devices.

2. Material and methods

*2.1 Materials and apparatus***.**

The β-D (+) glucose, chloroplatinic acid hydrate (H_2PtCl_6, purity: 99%), gold chloride hydrate ($HAuCl_4$, purity: 99%), ethanol, nitric acid (HNO_3) sodium chloride (NaCl), potassium chloride (KCl), isopropyl alcohol (IPA), chitosan (white mushroom, high molecular weight), Nafion (5%), ascorbic acid (AA), uric acid (UA), aliline, N-hydroxysuccinimide (NHS), and N-(3-dimethylaminopropyl)¬N-ethylcarbodiimide hydrochloride (EDC) were purchased from Aldrich Co. (St. Louis, USA). The β D (+) glucose solution was diluted in 0.05 M phosphate-buffered saline (PBS, pH 7.4) and allowed to stand for 24 h to allow equilibration. The Ag/AgCl paste was purchased from ALS Co., Ltd. (Japan). The hydrogen peroxide (H_2O_2) solution, AgNW, commercial polyimide film, and PDMS were purchased from 4science Co., Korea. Deionized (DI) water (resistivity: ≥18 MΩ ·cm) and 0.05 M PBS (pH 7.4) were used for all experiments.

2.2 Instrumentation.

The CO_2 laser (Model C30) was purchased from Coryart (Korea). Sensor patterns were designed in Autodesk Computer Aided Design (AutoCAD) software and used for CO_2 laser control. The stretchable electrode morphology was characterized by field emission scanning electron microscopy (FESEM). The physical characteristics of LIG were investigated by high-resolution X-ray photoelectron spectroscopy (XPS), Raman spectroscopy, and Fourier-transform infrared (FTIR) spectroscopy. Electrochemical characterization was performed at room temperature using a CH Instruments electrochemical analyzer (Model 660E, Austin, TX). A commercial glucose sensor was purchased from i-SENS. Inc. (Korea), and the portable electrochemical analyzer (Model PalmSen4) was purchased from Palmsens (The Netherlands).

2.3 Fabrication of stretchable electrodes.

The Stretchable electrodes (PDMS/AgNW/LIG) were fabricated by the flowing steps. First, LIG was directly written on the commercial polyimide (PI) film by using the computer-controlled CO_2 laser. After dipping in the 0.75 wt% AgNW, the film was dried at 80 °C for 20 min in a convection oven. Second, the liquid PDMS mixture was poured on the modified PI film. After a thermal curing at 90 °C for 60 min, the PDMS/AgNW/LIG slide was manually peeled off from the polyimide sheet. Third, the exposed AgNW (not covered by LIG) was etched by using 10 % HNO_3 solution for 1 min, the transferred LIG serves as protect mask layer of AgNW (under LIG layer). Finally, liquid PDMS mixture was cast on top of the electrode except sensing part.

2.4 Functionalization of glucose sensor with electrochemically active materials.

(i) Fabrication of the reference electrode. Ag/AgCl paste was cast on the PDMS/AgNW/LIG electrode and baked at 125 °C for 5 min in a convection oven. (ii) PtAuNP electrodeposition. The electrochemical deposition of AuPtNP was conducted using a potentiostatic configuration; AuPtNP was deposited on the PDMS/AgNW/LIG film of the working electrode in a 0.1 M KCl solution containing 1.0 mM H_2PtCl_6 and 1.0 mM $HAuCl_4$, respectively. The deposition potential was fixed at −0.2 V (vs commercial Ag/AgCl) and the deposition time was 300 s. In this case, both Au and Pt are reduced on the surface of the PDMS/AgNW/LIG electrode. During deposition, the solution was stirred with a magnetic bar and was maintained at room temperature. The fabricated electrodes were rinsed carefully with distilled water and then dried under nitrogen gas. (iii) glucose oxidase (GOx) layer immobilization. Approximately 3 µL of 40 mM EDC and 20 mM NHS mixing solution (water) was cast on the top of the modified working electrode and subsequently incubated for 7 h at room temperature. Next, 5 mg GOx and 2.5 mg chitosan were dissolved in 0.5 mL DI water, and 5 µL of the mixture was then cast onto the surface of the working electrode modified with the coupling agent. The solvent was subsequently allowed to dry in a refrigerator at 4 °C. Finally, 5 µL Nafion/ethanol solution (1:15) was dropped onto the working electrode and allowed to dry for 40 min at room temperature.

2.5 Functionalization of pH sensor with electrochemically active materials.

(i) Fabrication of the reference electrode. Ag/AgCl paste was cast on the PDMS/AgNW/LIG electrode and baked at 125 °C for 5 min in a convection oven. (ii) PANI electrodeposition. The PDMS/AgNW/LIG electrode was dipped into the in 1 M HCl solution with 0.1 M aniline, and the potential was swept from −0.2 to 1 V versus a commercial Ag/AgCl electrode for 60 segments at a scan

rate of 0.1 V s^{-1}. The fabricated electrodes were rinsed carefully with distilled water and then dried under nitrogen gas.

3. Results and discussion

3.1 Design and fabrication of the nanomaterial-based electrodes

Fig. 1a depicts the proposed concept for a human interactive wearable Chem-Phys sensor. A serpentine design was used to improve the deformability of the electrode. In the glucose-sensing part, the working electrode (WE), reference electrode (RE), and counter electrode (CE) are designed to be packed as closely as possible to minimize the sensor size for wearability (Fig. S1). As shown in Fig. 1b, a simple, low-cost fabrication process was used. The working electrodes (for glucose, pH and ECG sensors) consist of multiple layers (Fig. 1b inset, Fig. S2 and Fig. S3) to improve the electrical properties. The well-patterned AgNW layer decreases the sheet resistance of the electrode (in comparison to a previous Lamberti's work, increases the electron transfer property, and creates deformability that is accompanied by minimal resistance change (Fig. S4a and Fig. S4b). The 3D porous LIG layer above the AgNW allows for a larger surface area and stronger enzyme immobilization (Zhao et al., 2017; Singh et al., 2018). The PtAuNP layer, formed by electrodeposition with optimized conditions, improves the electron transfer rate at the interface and creates high H_2O_2-reducing catalytic activity (Barman et al., 2017; Shi et al., 2017). Finally, GOx enzyme was drop-cast onto the surface of the PtAuNP layer, sequentially cross-linked by N-(3-dimethylaminopropyl)-N-ethylcarbodiimide hydrochloride EDC/ N-hydroxysuccinimide (NHS), and covered by Nafion.

3.2 Physical characteristics of the modified LIG electrodes

Fig. 2a shows the FESEM images of the PDMS/AgNW/LIG electrode after transfer from the PI substrate using the technique described above (Fig. 1B). As a result of effective infiltration of PDMS, a well-patterned AgNW/LIG film was transferred onto the PDMS substrate. Moreover, as shown in Fig. 2b and Fig. 2c, a few interconnected multilayer LIG flakes are retained, while for the most part, 3D LIG and AgNW coexist with a PDMS matrix (Fig. S5). These results indicate successful impregnation by AgNW/LIG down to the bottom of the 3D structure. FESEM images of the PtAuNP on the AgNW/LIG electrode for different electrodeposition conditions are shown in Fig. 2d-2g. The

electrodeposition of PtAuNP was conducted using a potentiostatic configuration with a fixed potential of −0.2 V. These figures show that the PtAuNP is decorated over the 3D porous surface of the AgNW/LIG. The amount of PtAuNP deposited on the electrode surface increases with deposition time (Fig. 2d, 2e, and 2f are for 50, 150, and 300 s, respectively). As seen in Fig. 2f, for 300 s, the PtAuNP is well deposited on the surface of the deep porous LIG electrode. However, for longer times, the porous structure is blocked by over-deposition of the PtAuNP (Fig. 2g), reducing the surface area of the electrode. From this, we conclude that the optimal deposition time at −0.2 V is 300 s. The side view of the LIG/PtAuNP shown in the Fig. 2h shows that PtAuNP is present on both sides of the LIG.

Current-voltage characteristics (shown in Fig. 3a) were recorded for the LIG and AgNW/LIG layers on the PDMS substrate. The LIG (470 Ω) and Ag/LIG (130 Ω) electrodes demonstrate linear current-voltage curves. Meanwhile, the sheet resistance (R_s) of several electrodes was recorded in Table S1. The R_s of PI/LIG is 43 Ω/sq, reduced from a high value for PI alone, which is an insulator. With the AgNW coating, R_s is further reduced to 21 Ω/sq. After transfer to the PDMS substrate, the R_s values were increased to 98 Ω/sq (PDMS/LIG) and 30 Ω/sq (PDMS/AgNW/LIG). Lamberti et al. also reported a similar increase of R_s after transfer onto PDMS (24). These results indicate that AgNW/LIG can be transferred to the stretchable substrate and that AgNW improves the electrical properties. The Raman spectrum of LIG (Fig. 3b) contains three prominent peaks: the D peak at 1340 cm^{-1} (induced by defects or bent sp^2-carbon bonds), the G peak at 1600 cm^{-1}, and the 2D peak at 2690 cm^{-1} (originating from second-order zone-boundary phonons). The D/G intensity ratio indicates a high degree of graphene formation in the LIG electrode (Ferrari et al., 2006). The FTIR absorbance spectra (Fig. 3c) were recorded for LIG, PDMS, and LIG/PDMS; the spectrum for LIG does not show any peaks related to functional groups typically observed in GO-material, indicating a low number of defects in the graphenized PI. After transfer of the LIG to the PDMS, the FTIR spectrum of LIG/PDMS is very similar (peak positions and intensities) to PDMS alone. The XPS spectra of LIG and PDMS and their atomic percentages of elements are shown in Fig 3d-3g. The oxygen peaks in the LIG curves are significantly decreased in comparison with PDMS (Fig. 3d). High-resolution C1s XPS spectra for LIG and PDMS are shown in Fig. 3e; the C–O, C=O, O–C=O peaks are noted in the LIG spectrum. As seen from the high-resolution O1s XPS spectra of the Fig. 3f, the LIG peaks are greatly reduced in comparison to PDMS. These results indicate that the LIG films are well graphenized and transferred.

3.3 Electrochemical characteristics of of the modified LIG electrodes

Photographs of four different electrodes (the line-shaped and serpentine-shaped PDMS/LIG, line-shaped and serpentine-shaped PDMS/AgNW/LIG; labelled 1-4, respectively) are shown in Fig. 4a. The change in resistance for the four types subjected to stretching in the range 0-40% are shown in Fig. 4b. A line-shaped PDMS/LIG electrode (type 1) experiences a huge resistance change with stretching; this phenomenon may result from cracking of the LIG surface during stretching (Fig. 4c). After adding the AgNW film between the PDMS and LIG layers (type 2), the PDMS/AgNW/LIG line-shaped (type 3) and serpentine-shaped (type 4) electrodes show a dramatically reduced variation of resistance, even for an applied strain of up to 40%. This maximum strain is similar to that found in the human body, including the joints. This improvement of the stretchability in the type 4 electrode may have resulted from both the serpentine structure design and the AgNW layer between the PDMS and the LIG (Fig. S4). Cyclic voltammetry (CV) testing was conducted in order to evaluate the charge transfer behavior of the PDMS/LIG, PDMS/AgNW/LIG, and PDMS/AgNW/LIG/PtAuNP electrodes (Fig. 4d). For the PDMS/LIG electrode, a weak CV current was observed, indicating a low electron transfer rate at the interface. In contrast, an increased current is observed for the PDMS/AgNW/LIG electrode. The results indicate that AgNW improves the chemical properties of the electrode. This improved performance is attributed to the high conductivity of the AgNW. A significant increase in the peak current was observed at the PDMS/AgNW/LIG/PtAuNP electrode. This demonstrates that PtAuNP modification on the PDMS/AgNW/LIG/ surface increases the electroactive surface area of the modified electrode and accelerates electron transfer between the redox probe and electrode (Lee et al., 2018). The higher charge transfer rate of the PDMS/AgNW/LIG/PtAuNP electrode was further confirmed via electrochemical impedance spectroscopy (EIS) (Fig. 4e). It can be calculated that the R_{et} value decreases significantly with addition of AgNW and deposition of PtAuNP. This dramatic decrease in R_{et} can be primarily attributed due to an excellent electrical conductivity of both AgNW and PtAuNP, which promotes electron transfer from the electroactive markers to the electrode. Measurement of amperometric response of the stretchable electrodes (Fig. 4f), via the successive addition of glucose at regular time intervals, provides valuable information on sensitivity. The catalytic glucose oxidation capability of the electrodes can be evaluated using stepped current variations. A remarkable current increase is observed for the PDMS/AgNW/LIG/PtAuNP/GOx electrode, which is

highest compared with the other electrodes. This result indicates that AgNW and PtAuNP improve the electrochemical performance of the glucose sensor.

3.4 Electrochemical investigations of designed glucose sensor

The amperometric responses to H_2O_2 of PDMS/AgNW/LIG/PtAuNP electrodes fabricated using different electrodeposition times are compared in Fig. 5a; the response current increases as the deposition time is varied from 50 to 300 s. For a deposition time greater than 300 s (e.g., 450 s), the steady-state response current is slightly decreased. This may result from the decrease of active surface area (the 3D porous LIG was gradually filled by PtAuNP) with additional deposition time, which is confirmed by the FESEM image (Fig. 2g). The optimized deposition time of PtAuNP was therefore fixed at 300 s. The CV curves were obtained for the PDMS/AgNW/LIG/PtAuNP working electrodes using commercial and fabricated reference electrodes in a 0.1 M KCl solution containing 2 mM $K_3[Fe(CN)_6]$. The reference electrode was calibrated against a commercial Ag/AgCl (3 M KCl) electrode; from Fig. 5b, we can calculate that the standard potential shift is 150 mV compared to the normal hydrogen electrode. Furthermore, the current measured using the fabricated reference is not significantly different from that using the commercial reference. This indicates that the fabricated reference works well for electrochemical sensors. The effect of samples of some electrochemically activating molecules present in human sweat (5 µM uric acid (UA), 1 µM ascorbic acid (AA), 4 mM lactic acid (LA), 100 µM acetaminophen (Acetami.), and 0.1 mM NaCl) on the sensor response was investigated using an amperometric technique (Fig. 5c). In comparison to the reference signals from injected glucose droplets (first three injections are 0.1 mM; final injection is 0.2 mM), injections of these interfering molecules do not produce any significant signals, implying that the sensor exhibits good selectivity for glucose. The dependence of the sensor response on the test solution pH for glucose determination is shown in Fig. 5d; the pH value should be considered for an accurate measurement of glucose in sweat (pH range: 4–7). To investigate the use of a wearable glucose sensor for human sweat analysis, the wearable electrodes were connected to a portable electrochemical analyzer that supplies power and controls the sensor (Fig. S6). The portable analyzer could also communicate with commercial mobile devices wirelessly via Bluetooth. The stability of the biosensor was systematically evaluated by performing amperometric experiments over a period of one month (Fig. 5e). The wearable sensor was tested using 0.2 mM glucose (three repetitions per data point). The output signal of the first

experiment, S_0, was used to normalize subsequent experiments to evaluate sample stability (S_x/S_0). Within the initial 17 d, a stability >83% and relative standard deviations of 3.0−4.6% were obtained. However, by 17 d, the concentration of glucose oxidase in the sensor had gradually been reduced by prolonged usage and the relative sensitivity had decreased to 63%. These results indicate that the wearable sensor exhibits acceptable stability and repeatability. Fig. 5f displays amperometric data obtained directly from human sweat by using the wearable sensor. It can be clearly noted that the glucose sensor displays a distinct increment in the post-meal (blood glucose level: 133 mg/dl) current response as compared to the fasting state (blood glucose level: 91 mg/dl). This result indicates that the wearable biosensor design is suitable for the direct detection of glucose in sweat.

3.5 Performance of fabricated Chem-Phys hybrid biosensor

Chronoamperometry was used for sensing the glucose using the fabricated biosensor. The principle of the glucose sensor is schematically described in Fig. S7. The amperometric response of the glucose sensor (Fig. 6a) was also evaluated after the addition of glucose drops (concentrations: 5, 10, 50, 100, and 200 μM) into the phosphate-buffered saline (PBS) solution. The results displayed good linearity for different glucose concentrations (total addition: ~1.1 mM glucose). Ultimately, the suitable linear range of the sensor allows for the possibility of glucose detection in tears, saliva, and sweat (Liu et al., 2016). In Fig. 6d, the fabricated glucose sensor showed a correlation coefficient of 0.998 in the range 0–1.1 mM (glucose level range in human sweat) with high sensitivity (6.4 μA/(mM·cm^2)). Furthermore, the fabricated-sensor response reaches a steady-state within a few tens of seconds, even for a low concentration (limit of detection 5 μM). The pH sensor was fabricated for improve the accuracy of the glucose sensor. The pH sensor contains two electrodes; the PANI membrane coated electrode as a sensing electrode and the Ag/AgCl electrode as reference electrode. The schematic of the pH sensor is shown in Fig. S8. Fig. 6b shows a typical potential-time profile of the pH sensor on increasing and decreasing the pH level from 4 to 7 and 7 to 4. The sensor exhibited response potentials ranging from 51 to 255 mV on increasing pH from 4.0 to 7.0. The stable potential values obtained were plotted with respect to pH (Fig. 6e). The sensors provided a linear response of 66 mV/pH with a high correlation coefficient (R^2 = 0.999) across the pH range. The sensor showed a response time of 2 s. Furthermore, this experiment indicated that the reversibility of the sensors was good enough in the pH level range. The ECG signal was then measured using the PDMS/LIG and PDMS/AGNW/LIG

electrode without applying gel to the subject as shown in Fig. 6c, for a period of 14s. After the amplification, the ECG signal is processed by a band pass filter and an analog to digital converter (ADC). Finally, a finite impulse response (FIR) filter is used in Matlab to remove 60 Hz noises (Das et al., 2017). The obtained signals from PDMS/AGNW/LIG electrodes were stable and almost similar to that obtained from commercial Ag/AgCl electrode (3M). The experimental results show that the proposed PDMS/AGNW/LIG based dry electrode is able to operate in dry conditions when the subject is resting, which is comparable with traditional disposable gelled Ag/AgCl electrodes. It can be seen that the PQRST-wave appeared clearly in Fig. 6f, demonstrating that PDMS/AGNW/LIG based electrodes are capable of collecting good quality ECG signals which provide useful information about cardiovascular problems, with negligible fluctuation. In order to examine the ECG signal quality obtained from the proposed electrode, the signal to noise ratio (SNR) is calculated using the Wang reported equation (Wang et al., 2014). The SNR values are 5.71 dB for the Ag/AgCl, 0.49 dB for the PDMS/LIG and 0.61 dB for the PDMS/AGNW/LIG, respectively. Taking into account the SNR results, it can be stated that the performance of fabricated PDMS/AGNW/LIG electrode is better than the PDMS/LIG electrode. Because the conductivity of PDMS/AGNW/LIG electrode is greater than the PDMS/LIG electrode. The effect of the motion artifact on the ECG signal of the PDMS/LIG is greater than that on the ECG signal of the PDMS/AGNW/LIG and Ag/AgCl electrode. The PDMS/AGNW/LIG based ECG results is clearly observed to be stable and recognizable. However, the R-wave is clearly visible and detectable as shown in Fig. 6F. The obtained results proved that the ECG signal recorded by the PDMS/AGNW/LIG based electrode is similar to the Ag/AgCl electrode.

4. Conclusion

In summary, we have successfully fabricated a Chem-Phys biosensor using LIG based electrodes on a stretchable substrate, based on a novel fabrication process (inexpensive and simple), material structure, and sensor design. The glucose sensor (with acceptable selectivity, long time stability, and sensitivity), pH sensor (improving the accuracy of the glucose sensor), and ECG sensor using modified LIG electrodes have been successfully demonstrated. Depending on the design, the stretchable and small-scale patternable electrodes (PDMS/AgNW/LIG) and 3D porous nano-material structures (LIG/PtAuNP) can be used in various wearable electronics including sensors and energy storage. In the

near future, we are supposed to integrate this device with a flexible printed circuit board in order to implement a highly miniaturized smart health care monitoring system.

Acknowledgements

This research was supported by the Bio & Medical Technology Development Program of the NRF grant funded by the Korean government (MSIT) (NRF-2017M3A9F1031270). The authors are grateful to MiNDaP (Micro/Nano Device & Packaging Lab) group members at the Department of Electronic Engineering, Kwangwoon University, for their technical discussion and support.

Author contributions

X. X. discovered the process, designed, performed, analyzed, and wrote the manuscript. X. X., X. H. and J. Y. K. helped to fabricate the hybrid electrodes. X. X. and X. H. designed and performed the electrochemical experiments and analysis. P. S. D. performed the ECG experiments and analysis. X. X. and Y. S. Y. managed and discussed to draw and plot all the figures. Finally, J. Y. P. advised all research phases, provided technical guidance, and revised the manuscript.

Additional Information

Competing financial interests: The authors have no competing financial interests to declare.

References

Bandodkar, A. J., Molinnus, D., Mirza, O., Guinovart, T., Windmiller, J. R., Valdés-Ramírez, G., Andrade, F. J., Schöning, M. J., Wang, J., 2014. Biosensors and Bioelectronics. 54, 603–609.

Barman, S. C., Hossain, M. F., Park, J. Y., 2017. Journal of The Electrochemical Society, 164, B234-B239

Cai, F., Yi, C., Liu, S., Wang, Y., Liu, L., Liu, X., Xu, X., Wang, L., 2016. Biosensors and Bioelectronics. 77, 907-913.

Chen, C., Ran, R., Yang, Z., Lv, R., Shen, W., Kang, F., Huang, Z., 2018. Sensors and Actuators B: Chemical. 56, 63–70.

Cho, B., Kim, A. R., Kim, D. J. Chung, H., Choi, S. Y. Kwon, J., Park, S. W. Kim, Y., Lee, B. H., Lee, K. H., Kim, D., Nam, J., Hahm, M. G., 2016. ACS Applied Materials & Interfaces. 8, 19635−19642.

Das, P., Park J., 2017. Biomedical Signal Processing and Control 33, 72–82

Ferrari, A. C., Meyer, J. C., Scardaci, V., Casiraghi, C., Lazzeri, M., Mauri, F., Piscanec, S., Jiang, D., Novoselov, K. S., Roth, S., Geim, A. K., 2006. PRL, 97, 187401.

Gao, W., Emaminejad, S., Nyein, H. Y. Y., Challa, S., Chen, K., Peck, A., Fahad, H. M., Ota, H., Shiraki, H., Kiriya, D., Lien, D., Brooks, G. A. Davis, R. W., Javey, A., 2016. NATURE. 529,509.

Guo, H., Lan, C., Zhou, Z., Sun, P., Wei, D., Li, C., 2017. Nanoscale. 9, 6246.

Kwak, Y. H., Kim, W., Park, K. B., Kim, K., Seo, S., 2017. Biosensors and Bioelectronics. 94, 250-255.

Lamberti, A., Clerici, F., Fontana, M., Scaltrito, L., 2016. ADVANCED ENERGY MATERIALS. 6, 1600050.

Lee, H., Hong, Y., Baik, S., Hyeon, T., Kim, D., 2018. Adv. Healthcare Mater. 1701150

Lee, H., Song, C., Hong, Y. S., Kim, M. S., Cho, H. R., Kang, T., Shin, K., Choi, S. H., Hyeon, T., Kim, D., 2017. SCIENCE ADVANCES. 3, e1601314.

Lei Shi, L., Wang, Y., Ding, S. M., Chu, Z. Y., Yin, Y., Jiang, D. F., Luo, J. Y., Jin, W. Q., 2017. Biosensors and Bioelectronics. 89, 871-879.

Li, J., Delekta, S. S., Zhang, P., Yang, S., Lohe, M. R., Zhuang, X., Feng, X., O□stling, M., 2017. ACS Nano. 11, 8249−8256.

Lin, J., Peng, Z., Liu, Y., Ruiz-Zepeda, F., Ye, R., Samuel, E. L.G., Yacaman, M. J., Yakobson, B. I., Tour, J. M., 2014. NATURE COMMUNICATIONS. 5:5714.

Liu, J., Sun, S., Shang, H., Lai, J., Zhang, J., 2016. Electroanalysis 28, 2016–2021

Liu, Y., Pharr, M., Salvatore, G. A. 2017. ACS Nano. 6, 3702–3708.

Maharjan, P., Toyabur, R.M., Park, J. Y., 2018. Nano Energy. 46, 383-395.

Matzeu, G., Florea, L., Diamond, D., 2015. Sensors and Actuators B: Chemical. 211, 403–418.

Moyer, J., Wilson, D., Finkelshtein, I., Wong, B., Potts, R., 2012. DIABETES TECHNOLOGY & THERAPEUTICS. 5, 14.

Olarte, O., Chilo, J., Pelegri-Sebastia, J., Barb´e, K., Moer, W. V., 2013. IEEE EMBS. 1, 1462-1465.

Pang, Y., Jian, J., Tu, T., Yang, Z., Ling, J., Li, Y., Wang, X., Qiao, Y., Tian, H., Yang, Y., Ren, T., 2018. Biosensors and Bioelectronics. 116, 123–129.

Pegan, J. D., Zhang, J., Chu, M., Nguyen, T., Park, S., Paul, A., Kim, J., Bachman, M., Khine, M., 2016. Nanoscale. 8, 17295.

Roy, S., David-Pur, M., Hanein, Y., 2017. ACS Applied Materials & Interfaces. 9, 35169−35177.

Singh, S., Li, Y., Zhang, J., Tour, J. Arnusch, J., 2018. ACS Nano 12, 289−297

Tao, L., Tian, H., Liu,Y., Ju, Z., Pang, Y., Chen, Y., Wang, D., Tian, X., Yan, J., Deng, N., Yang, Y., Ren, T., 2017. NATURE COMMUNICATIONS. 8:14579.

Wang, L., Liu, J., Dong, Y., Yang, B., Chen, X., Yang C., 2014. Sensors and Actuators B. 205, 168–175.

Wang, Z., Gui, M., Asif, M., Yu, Y., Dong, S., Wang, H., Wang, W., Wang, F., Xiao, F., Liu, H., 2018. Nanoscale, 10, 6629.

Xuan, X., Park, J. Y., 2018. Sensors and Actuators B: Chemical. 255, 1220-1227.

Xuan, X., Yoon, H. S., Park, J. Y., 2018. Biosensors and Bioelectronics. 109, 75–82.

Yamamoto, Y., Harada, S., Yamamoto, D., Honda, W., Arie, T., Akita, S., Takei, K., 2016. SCIENCE ADVANCES. 2, e1601473.

Zhao, Q., Zhao, M., Qiu, J., Lai, W., Pang, H., Huang, W., 2017. Small 13, 1701091

Fig. Captions

Fig. 1. Conceptual drawing, optical images and fabrication process of the wearable Chem-Phys sensor. (**a**) Conceptual image of the wearable glucose sensor band and photographs of a wearable sensor. (b) The detail fabrication process of stretchable electrodes and the schematic drawing of multilayered working electrodes (inset).

Fig. 2. FESEM images of PDMS/AgNW/LIG and PDMS/AgNW/LIG/PtAuNP nanocomposite electrodes. (a), (b) FESEM images of PDMS/AgNW/LIG surface (top view). Note different magnifications. (c) Side view of PDMS/AgNW/LIG electrode. (d), (e), (f), and (g) FESEM images of PDMS/AgNW/LIG/PtAuNP for different electrodeposition times (50, 150, 300, and 450 s, respectively). (h) Side view of PDMS/AgNW/LIG/PtAuNP.

Fig. 3. Electrical and physical characterization of AgNW/LIG and AgNW/LIG electrodes. (a) Current-voltage characteristics of LIG and AgNW/LIG electrodes. (b) Raman spectrum of a LIG and PDMS. (c) FTIR spectra of PDMS and LIG. XPS characterization of LIG and PDMS (d) wide scan, (e) C 1s spectra, and (f) O 1s spectra. (g) Summary of atomic percentage of elements in PDMS and LIG.

Fig. 4. Electrochemical and electrical characterization of fabricated stretchable electrodes. (a) As-prepared LIG based electrodes. PDMS/LIG-line type (1), PDMS/LIG-serpentine type (2), PDMS/AgNW/LIG-line type (3), PDMS/AgNW/LIG-serpentine type (4), (b) Resistance change of each electrode (1-4 of panel (A)) under stretching of up to 40 %. (c) FESEM image of the crack of electrode (during the stretching). (d) CV curves of LIG (black line), as compared to AgNW/LIG (red line) and AgNW/LIG/PtAuNP (blue line) in 100 mM KCl solution containing 2mM $K_3[Fe(CN)_6]$. (e) EIS of the LIG (green line), as compared to LIG/PtAuNP (blue line), AgNW/LIG (red line) and AgNW/LIG/PtAuNP (black line) in 100 mM KCl solution containing 2mM $K_3[Fe(CN)_6]$. (f) The amperometric responses of the several stretchable electrodes PDMS/LIG/PtAuNP (black line), as

compared to PDMS/LIG/GOx (red line) and PDMS/AgNW/LIG/PtAuNP/GOx (blue line) in PBS solution.

Fig. 5. Electrochemical characterization of the fabricated wearable glucose sensor. (a) Amperometric curves of PDMS/AgNW/LIG/PtAuNP electrode at various deposition time of 0sec, 50sec, 150sec, 300sec and 450sec in 0.05 mM PBS solution (1 mM H_2O_2 injection at 300 sec). (b) Cyclic voltammograms of the fabricated reference electrode and commercial Ag/AgCl (3 M KCl) electrode in 0.1 M KCl solution containing 2 mM $K_3[Fe(CN)_6]$. Scan rate: 50 mV/s. (c) Selectivity experiment using amperometric current responses of the biosensor with successive addition of 0.1 mM glucose (twofold), followed by 5 µM U. A., 0.1 M NaCl, 1 µM A. A., 0.2 mM glucose, 4 mM L. A., 100 µM Acetami., and finally 0.2 mM glucose in 0.05 M PBS solution. (d) Changes of the relative current responses of the fabricated wearable biosensor at different pH levels (glucose concentration: 0.2 mM). (e) Stability (compare to the value of the first test) of the fabricated biosensor (repeated amperometric experiments were conducted for one month). (f) Amperogram for glucose detection obtained from human sweat directly (inset: wide current range).

Fig. 6. Performance characterization of the fabricated wearable hybrid bio-sensor. (a) Amperometric current responses with successive addition of different glucose concentrations (50 µM, 100 µM, 200 µM). inset: detection limit. (d) calibration curve through linear fitting (from Fig. 6A). (b) Repeatability test for pH sensor with varying pH levels in a range of 4 to 7 (the sweat pH range). (e) Potential values versus pH values for sensor. (c) ECG signal measured when the subject was resting after FIR filtering in Matlab using (black) Ag/AgCl, (blue) PDMS/LIG and (red) PDMS/AgNW/LIG. (f) Comparison of the PQRST waves among the (black) Ag/AgCl, (blue) PDMS/LIG and (red) PDMS/AgNW/LIG.

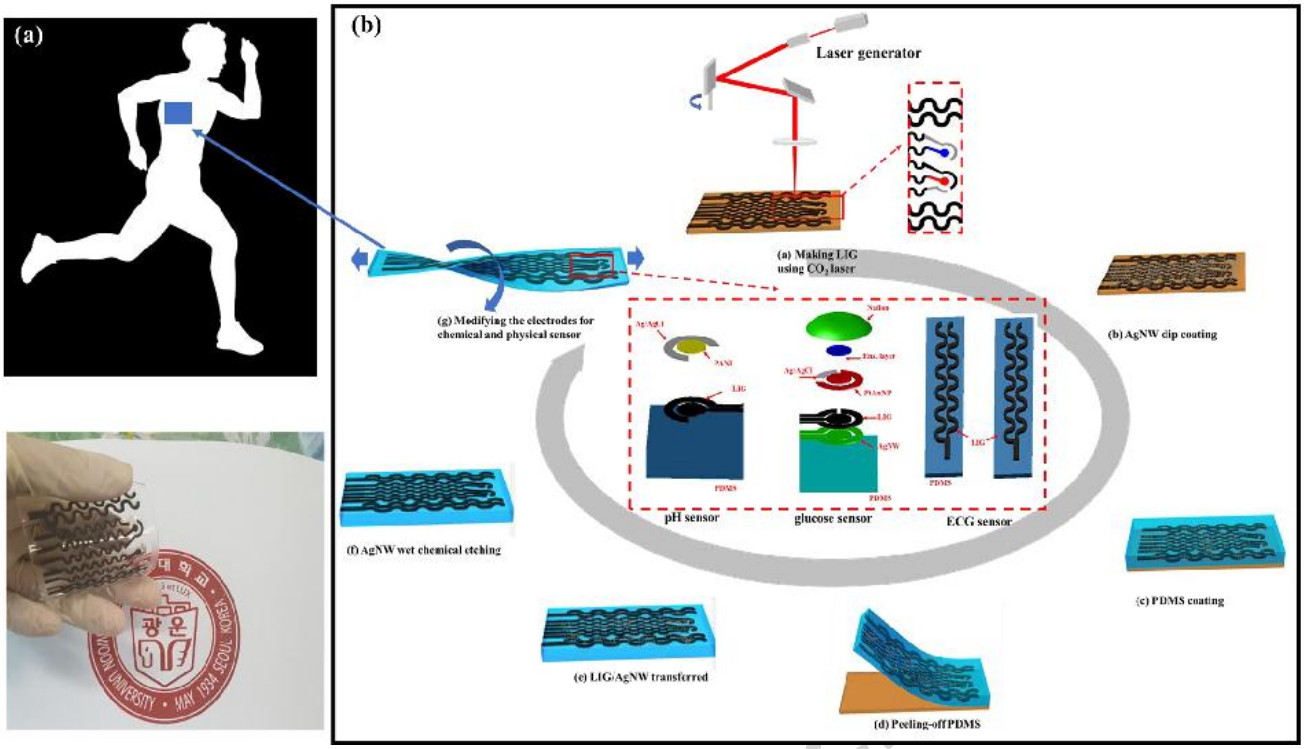

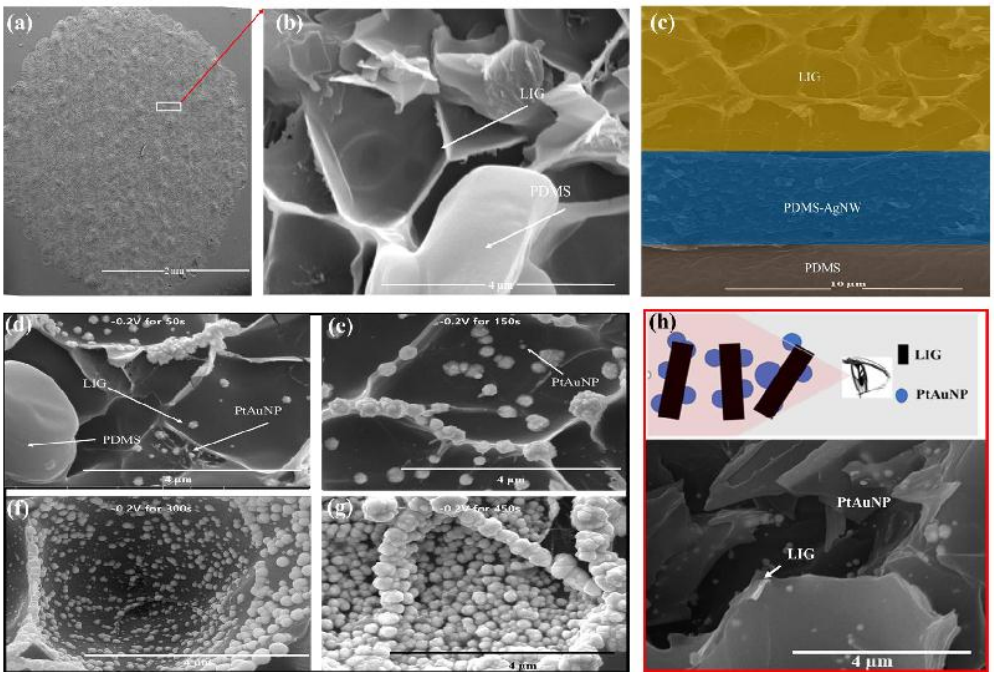

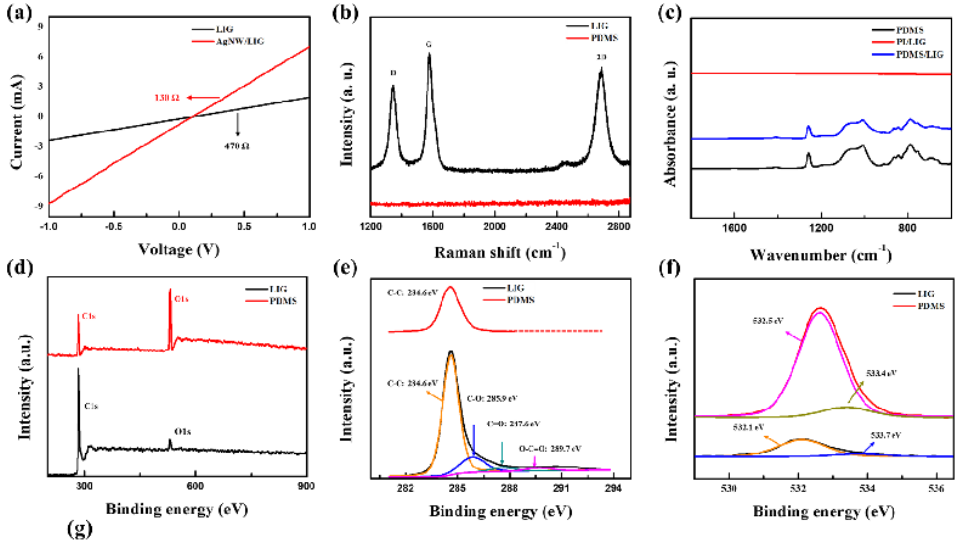

(g)

Materials	Carbon (%)	Oxygen (%)	Nitrogen (%)
PDMS	43.9	26.6	29.5
LIG	93.8	2.25	3.95

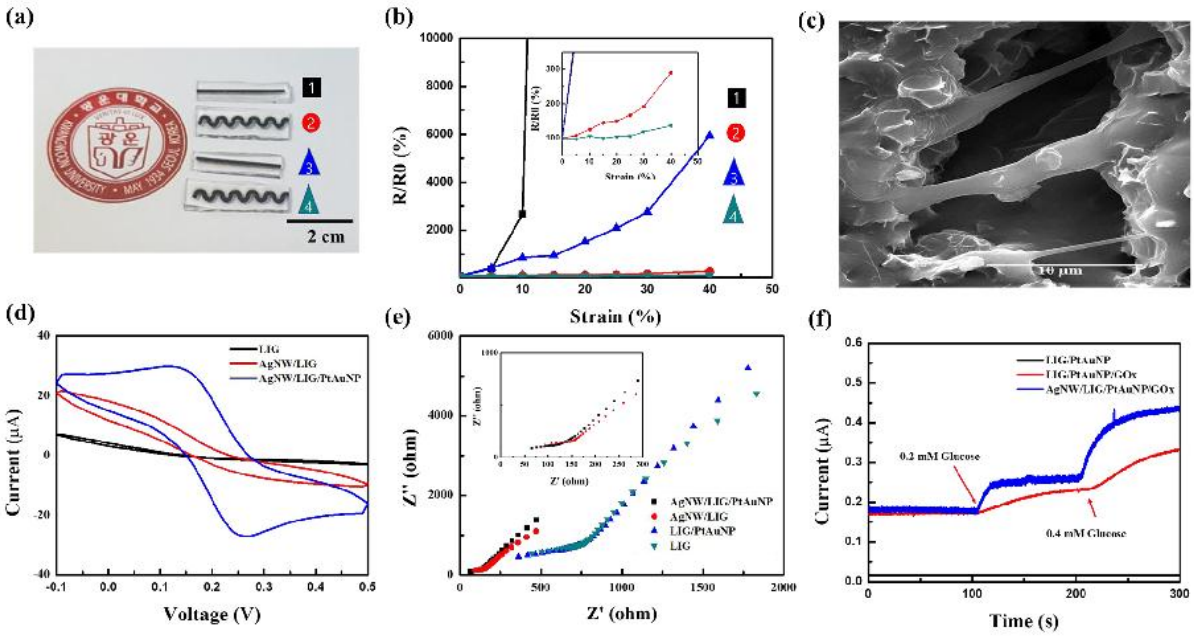

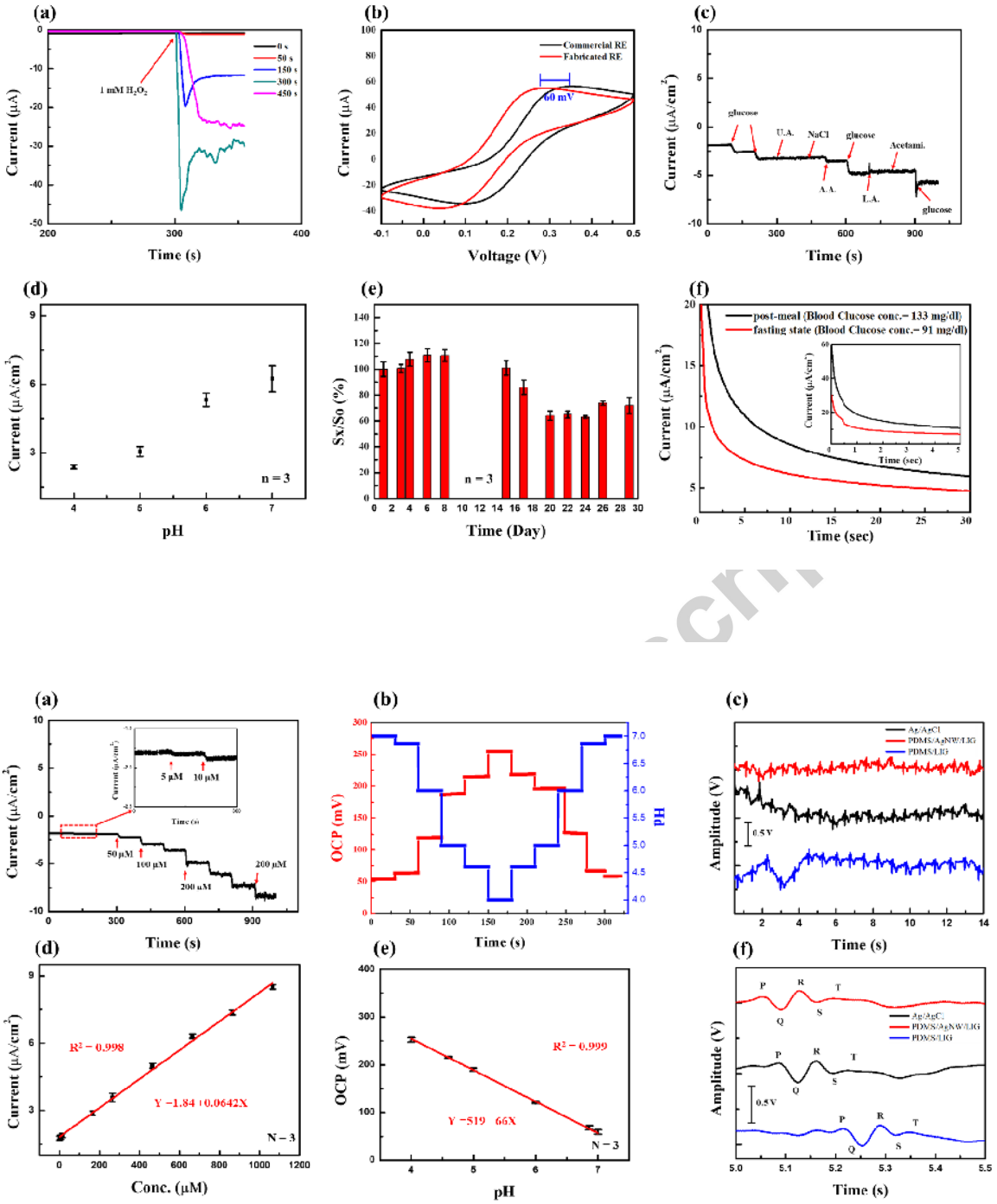

Highlights

- A novel fabrication process (both inexpensive and simple) for the highly stretchable and conductive electrodes using well patterned 3D porous laser-induced graphene (LIG) silver nanocomposite was developed, the

fabricated electrodes exhibit a high, uniform electrical conductivity even under mechanical deformations.

- Platinum and gold nanoparticles (PtAuNP) were deposited on the 3D porous LIG and it greatly improves the electrochemical performance for wearable sensor applications.
- Human sweat samples were used and acceptable results were obtained using electrochemical-physiological hybrid biosensors.